Enhancement of methylmercaptan sensing response of WO_3 semiconductor gas sensors by gas reactivity and gas diffusivity

Taro Ueda[1], Takuya Maeda[1], Zhendong Huang[1], Kotono Higuchi[1],

Kuniyuki Izawa[2], Kai Kamada[1], Takeo Hyodo[1] and Yasuhiro Shimizu[1]

[1]Graduate School of Engineering, Nagasaki University,

1-14 Bunkyo-machi, Nagasaki 852-8521, Japan

[2] Figaro Engineering Inc.,

1-5-11 Senbanishi, Minoo, Osaka 562-8505, Japan

*Corresponding author:
Taro Ueda, Dr.
Graduate School of Engineering, Nagasaki University
1-14 Bunkyo-machi, Nagasaki 852-8521, Japan
Tel: +81-95-819-2645
Fax: +81-95-819-2643
E-mail: taroueda@nagasaki-u.ac.jp

Abstract

WO_3-based semiconductor-type gas sensors were fabricated, and their sensing properties to methylmercaptan (CH_3SH) were examined in this study. The Ru loading on WO_3 was an effective way of an increase in the CH_3SH response. In addition, the CH_3SH response increased with a decrease in the operating temperature as well as with an increase in the thickness of the Ru-loaded WO_3 sensing layer. The increase in the porosity of the Ru-loaded WO_3 sensors, which were fabricated by utilizing polymethylmethacrylate microspheres as a template, was also effective in improving the CH_3SH response, especially at a low temperature of 150°C. In addition, the lamination of the Ru-loaded WO_3 sensor with an α-Al_2O_3 film improved the CH_3SH response at 200°C. Moreover, the Ru loading on the WO_3 powder increased the catalytic activities of CH_3SH oxidation, and CH_3SH was partially oxidized to CH_3SSCH_3 at temperatures less than 330°C. It was suggested that the increase in the positively charged adsorption of the partially oxidized products onto the bottom part of the sensing layer is effective for enhancing the CH_3SH response, especially at lower operating temperatures.

***Keywords*:** semiconductor-type gas sensor; CH_3SH; Ru-loaded WO_3; CH_3SSCH_3, positively charged adsorption;

Introduction

Exhaled breath of the patients contains a higher concentration of specific gases than those of healthy people. For example, the patients suffering from lung cancer, diabetes and malfunctioning of liver and/or kidney release a high concentration of toluene, acetone and ammonia, respectively [1–3]. Therefore, the highly sensitive and selective analyses of gaseous components in the exhaled breath by utilizing gas-sensing devices are quite useful in diagnosing these diseases non-invasively. Among various kinds of gas sensors, semiconductor-type gas sensors have been widely studied because of the advantages of a simple structure, low fabrication cost, and rather easy customization for the detection of specific gases [4–6].

Halitosis of the patients suffering from periodontitis contains a high concentration of various volatile sulfur compounds (VSCs), such as hydrogen sulfide (H_2S) and methyl mercaptan (CH_3SH), and the formation of large periodontal pockets between gums and teeth increases the percentage of CH_3SH in the exhaled breath [7]. Therefore, sensitive and selective detection of CH_3SH is necessary to evaluate periodontal disease accurately.

Many researchers have attempted to develop highly selective and sensitive semiconductor-type VSCs sensors, but there are only a few reports on the detection of CH_3SH [8–12]. On the other hand, most of them have focused on the detection of H_2S. In particular, WO_3 is well known as one of the attractive sensing materials, and the loading of a small amount of metal onto WO_3 was quite effective in improving H_2S-sensing properties [13–20]. For example, Shen et al. reported that the optimal deposition of Pt on the surface of a WO_3 sensor effectively enhanced the H_2S response [17]. Yin et al. showed that the surface modification of WO_3 nanoplates with Au-loaded SnO_2 nanocrystals drastically improved the sensing properties to H_2S [18]. Lee et al. reported that nanosized oxide particles such as ZnO, SnO_2 and WO_3 sensitively detected H_2S and concluded that 0.01 wt% Au-loaded WO_3 was the most suitable material for the detection of sub-ppm H_2S [19]. Quite recently, Kruefu et al. reported that Ru loading onto WO_3 improved the sensor response to sub-ppm H_2S together with improved response and recovery behavior and the sensor showed the selective H_2S

response against NO_2, SO_2, C_2H_5OH and NH_3 [20].

In addition, thickness and porosity of the sensing layer are well known as important factors in determining gas-sensing properties of semiconductor-type gas sensors [21–29]. For example, we have actually reported that the porous metal oxides (e.g., In_2O_3 or SnO_2) prepared by utilizing a self-assembly of surfactants such as *n*-cetylpyridinium chloride (several nm in diameter) or polymethylmethacrylate (PMMA) microspheres (28–1500 nm in diameter) as a template showed excellent gas-sensing properties, due to the enhancement of both the gas diffusivity and the gas reactivity on their oxide surface [25–29].

We therefore focused on WO_3 as a CH_3SH-sensing material of semiconductor-type gas sensors, and discussed the effects of Ru loading onto WO_3 on the CH_3SH-sensing properties in this study. In addition, we also examined the effects of introducing a porous structure using PMMA microspheres into the sensing layer or laminating a catalytic layer onto the sensing layer on the CH_3SH response of the sensors. The impacts of catalytic activity of WO_3-based powders for CH_3SH oxidation on their CH_3SH response were also discussed in this study.

Experimental

2.1 Preparation of WO_3 powders loaded with and without Ru

HNO_3 aq. (0.10 mol dm^{-3}) was added dropwise into a Na_2WO_4 aqueous solution (0.15 mol dm^{-3}), and then the yellow resultant precipitate was calcined at 400–700°C for 2 h in air. It was confirmed that the crystal structure of the prepared powders, which was investigated by X-ray diffraction analysis (XRD; Rigaku Corp., RINT2200) using Cu Kα radiation (40 kV, 36 mA), was monoclinic WO_3 (JCPDS No. 43-1035). In addition, the specific surface area (SSA) was measured by the Brunauer-Emmett-Teller (BET) method using a N_2 adsorption isotherm (Micromeritics Inst. Corp., TriStar 3000). The as-prepared WO_3 powders were impregnated in aqueous solution dissolving an appropriate amount of $RuCl_3$ with ultrasonic treatment. After the solvent was evaporated to dry the mixtures at 100ºC, the obtained powders were heat-treated in H_2 at 200ºC for 2 h. The obtained Ru-loaded WO_3 powders were denoted as *n*Ru/WO_3 (*n*: the loading amount of Ru (wt%)). These powders

were heat-treated at 500°C for the fabrication of the sensors (see the next section), and the loaded Ru components were confirmed to be RuO_2 by X-ray photoelectron spectroscopy using Al Kα radiation (XPS, Kratos Analytical Ltd., ACIS-TLATRA DLD), the data is not shown here).

2.2 Fabrication of thick film sensors and measurement of their gas-sensing properties

The obtained *n*Ru/WO_3 powder was mixed with the same weight of α-terpineol, and the obtained paste was screen-printed onto the sensor substrate equipped with a pair of interdigitated Pt electrodes (gap size: ca. 100 μm), followed by drying at 100ºC. Porous-structured oxide layers were prepared by applying the paste mixed with an appropriate amount of PMMA microspheres (Soken Chem. & Eng. Co., Ltd., MP1000, ca. 400 nm in diameter). The same kind of paste was repeatedly over-coated on the dried green film, to increase the thickness. Only the thickest sensing layer (thickness: ca. 50 μm) was fabricated by applying the paste with a wooden pick. Then, Pt wires were attached onto the edge of the electrodes, followed by heat treatment at 500ºC for 2 h. The *n* wt% Ru-loaded WO_3 sensors fabricated were denoted as *n*Ru/WO_3(*T,t*) (*T*: calcined temperature of WO_3, *t*: thickness of the sensing layer (μm)). The porous *n*Ru/WO_3 sensors fabricated by employing the PMMA microspheres were denoted as p-*n*Ru/WO_3(*T*,*t*). In some cases, Al_2O_3 powders (α-Al_2O_3; Taimei Chemicals Co., Ltd., TM-DAR, SSA: 15 m^2 g^{-1}) or *m* wt% Pd-loaded Al_2O_3 (*m*Pd/α-Al_2O_3) powders, which were prepared by impregnation method [30], were mixed with an appropriate amount of α-terpineol, and they were laminated by applying on the sensing layer as a catalytic layer. The *0.5*Ru/WO_3(*500,20*) sensors laminated with the catalytic layer were denoted as M//N//*0.5*Ru/WO_3(*500*,*20*) or N//*0.5*Ru/WO_3(*500*,*20*) (*m*: the loading amount of Pd (wt%), M//N or N: catalytic layer, M: *m*Pd/α-Al_2O_3 upper layer, N: α-Al_2O_3 (under layer).

The microstructural images of the fabricated sensors were obtained by scanning electron microscopy (SEM; JEOL Ltd., JSM-7500F). Gas responses of these sensors were measured to 0.5 ppm CH_3SH balanced with wet air (65%RH at 20°C) at temperatures of 200–400°C, which were controlled by using a Pt heater on the back side of the sensor substrate. The CH_3SH response ($R_s = R_a/R_g$) was defined as the ratio of sensor's resistance in air (R_a) to that in the target gas (R_g).

2.3. Evaluation of catalytic combustion behavior of CH_3SH over sensing materials

The WO_3 or *0.5*Ru/WO_3 powder was pressed into disc, and then crushed into granules (ca. 20–60 mesh). The granules of about 0.6 g, which were fixed in a glass reactor of the flow apparatus, were exposed to 80 ppm CH_3SH balanced with wet air (65%RH at 20°C), at a flow rate of 30 cm^3 min^{-1} (a gas hourly space velocity (GHSV) of 5560 h^{-1}). The catalytic combustion behavior of CH_3SH over WO_3 or *0.5*Ru/WO_3 powders was then evaluated in the temperature range of 30–400°C, by using a gas chromatography mass spectrometer (GC-MS; Shimadzu Corp., QP-5500,).

Results and discussion

Figures 1 (a)–(e) show cross-sectional SEM photographs of the sensing layers of representative *0.5*Ru/WO_3(*500*,*t*) sensors, together with their thickness. The thickness of the sensing layer increased with an increase in the number of screen printing, and the thickness of the sensing layer fabricated by application was larger than those of the sensing layer fabricated by the screen printing. The thickness of the sensing layer was controlled in a range of 5–50 μm. A surface SEM photograph of only the *0.5*Ru/WO_3(*500*,*32*) sensor as a representative was shown in Fig. 1 (f). Large submicron-sized cracks were observed on the surface, probably due to sintering among WO_3 nanoparticles during the heat treatment after the screen printing, and the each flake-like sensing layer was rather uniform, consisting of well-developed pores with a diameter of less than 100 nm.

Figure 2 shows effects of the thickness of the sensing layer of the *0.5*Ru/WO_3(*500*,*t*) sensors on the magnitude of response to 0.5 ppm CH_3SH at operating temperatures of 200, 300 and 400°C. The magnitude of response at 400°C was the smallest over the whole thickness range examined, and the response at 400°C slightly decreased with an increase in the thickness. The CH_3SH response at 300°C was larger than that at 400°C, and the value was the largest when the thickness was ca. 15 μm. On the other hand, the CH_3SH response increased with an increase in the thickness of the sensing layer at 200°C, and it saturated over 30 μm in thickness. Figure 3 shows response transients of the *n*Ru-WO_3(*500*,*20*) sensors to 0.5 ppm CH_3SH in wet air at 200, 300 and 400ºC. The Ru-unloaded

WO_3(*500*,*20*) sensor (namely, *0*Ru-WO_3(*500*,*20*) sensor) showed quite a low resistance, and the loading of Ru on WO_3 increased the sensor resistance values in base air at all temperatures, because the concentration of electrons in WO_3 decreased due to the electron transfer from WO_3 to Ru-based components (RuO_2 in this case) [31, 32]. Introduction of CH_3SH into wet air decreased resistance values of all the sensors, and then the CH_3SH response increased with an increase in the amount of Ru loading at 200°C and 300°C while the CH_3SH response decreased with an increase in the amount of Ru loading at 400°C. In addition, the *n*Ru/WO_3(*500*,*20*) sensors (*n=0.10*, *0.25*) showed the largest CH_3SH response at 300°C, while the CH_3SH response of the *0.5*Ru/WO_3(*500*,*20*) sensor decreased with an increase in the operating temperature. Among them, the *0.5*Ru/WO_3(*500*,*20*) sensor exhibited the largest CH_3SH response at 200°C. Figure 4 shows calcination-temperature dependence of the CH_3SH response of the *0.5*Ru/WO_3(*T*,*t*) sensors at 200°C and SSA of the *0.5*Ru/WO_3 powders, together with the thickness of their sensing layers. The magnitude of responses was less dependent on the calcination temperature in the range of 500–700°C, while the response at 400°C was larger than those at 500–700°C. The SSAs of the *0.5*Ru/WO_3 powders increased with a decrease in the calcination temperature, and the SSA of the *0.5*Ru/WO_3 powder calcined at 400°C was much larger than those calcined at 500–700°C. The thickness of the sensing layer increased with a decrease in the calcination temperature. This is because that lower calcination temperature does not accelerate sintering among WO_3 particles and then maintains porous structure.

The thickness of the sensing layer is quite an important factor in controlling the gas-sensing properties of semiconductor-type gas sensors. In the case of the thick film semiconductor n-type gas sensors designed for VOC gas detection, the most sensitive region in the bottom part of the sensing layer close to interdigitated electrodes on the substrate [14]. Thus, the diffusivity and reactivity of CH_3SH in the sensing layer are quite important to determine the magnitude of the response, because the actual concentration of CH_3SH and the partially oxidized products (namely, chemical species which can react with negatively adsorbed oxygen) at the bottom part of the sensing layer is largely dependent on them. Actually, Figs. 2–4 show that the loading of Ru onto WO_3, the decrease in the operating temperature, the increase in the thickness of the sensing layer and the increase in the SSA

of *n*Ru/WO_3 powders obviously enhanced the CH_3SH response.

Catalytic combustion behavior of 80 ppm CH_3SH over WO_3 and *0.5*Ru/WO_3 powders in wet air was investigated as shown in Fig. 5, to clarify the reactivity of CH_3SH in the sensing layer. CH_3SH was oxidized over both the powders even at temperatures less than 100°C, and the catalytic activity of *0.5*Ru/WO_3 was higher than that of WO_3 especially in the temperature range of 75–200°C. Most of CH_3SH was oxidized over both the powders at temperatures higher than 250°C. In addition, the amount of dimethyl disulfide (CH_3SSCH_3, one of partially oxidized products) increased with an increase in CH_3SH conversion of both the powders. The largest amount of CH_3SSCH_3 generated at around 175°C and 125°C for WO_3 and *0.5*Ru/WO_3 powders, respectively. In addition, the amount of CH_3SSCH_3 generated over the *0.5*Ru/WO_3 powder was larger than that over the WO_3 powder in a wide temperature range. Furthermore, SO_2 was generated for both the powders at temperatures higher than 200°C, and the amount of SO_2 tended to increase with a rise in temperature. In addition, CH_3SSCH_3 was hardly produced at over 350°C for both the powders. This indicates that CH_3SH was completely oxidized at elevated temperatures.

On the basis of the results of catalytic activities of WO_3 and *0.5*Ru/WO_3 powders for CH_3SH oxidation, a possible CH_3SH-sensing mechanism of the sensors is illustrated in Fig. 6. Generally, the CH_3SH response of this type of sensors arises from the resistance change at the bottom part of the sensing layer between interdigitated Pt electrodes. The sensor resistance probably decreases with a decrease in negatively adsorbed oxygen consumed by the reaction with CH_3SH (oxidation of CH_3SH) and with an increase in positively charged adsorption of CH_3SH and/or the partially oxidized products such as CH_3SSCH_3 onto the oxide surface at the bottom part of the sensing layer, when CH_3SH was induced into base air. The amount of CH_3SH oxidized in the surface region of the sensing layer probably increased with a rise in temperature, due to the temperature-dependent catalytic activity. Since only a small amount of CH_3SH can reach to the bottom part of the sensing layer at elevated temperatures, the response of all the *0.5*Ru/WO_3(*500*,*t*) sensors is really small at 400°C, as shown in Fig. 2. On the other hand, the amount of CH_3SH which can reach to the bottom part of the sensing layer decreased with an increase in the thickness of the sensing layer, as the given amount of CH_3SH

is oxidized in the surface region of the sensing layer increased. Therefore, the CH_3SH response of the *0.5*Ru/WO_3(*500*,*t*) sensors slightly decreased with an increase in the layer thickness at 400°C (see Fig. 2). The amount of CH_3SH completely oxidized in the surface region of the sensing layer at 300°C is much smaller than that at 400°C (see Fig. 5), and thus the amount of CH_3SH which can reach to the bottom part of the sensing layer is expected to increase. In addition, CH_3SSCH_3 slightly produced as a partially oxidized product in the surface region of the sensing layer, as shown in Fig. 5. These results indicate that both CH_3SH and CH_3SSCH_3 react with negatively adsorbed oxygen and positively adsorbed on the bottom part of the sensing layer and thus the magnitude of CH_3SH response of all the *0.5*Ru/WO_3(*500*,*t*) sensors at 300°C is larger than that of 400°C. Furthermore, the *0.5*Ru/WO_3(*500*,*15*) sensors showed the largest CH_3SH response at 300°C, probably because the consumption of negatively adsorbed oxygen by the reaction with CH_3SH and CH_3SSCH_3 and positively charged adsorption of CH_3SH and CH_3SSCH_3 synergistically made the largest contribution toward the decrease in the sensor resistance at the medium temperature. The CH_3SH response of the *0.5*Ru/WO_3(*500*,*t*) sensors largely increased with an increase in the thickness of the sensing layer at 200°C. This is probably due to the lower catalytic activity for CH_3SH oxidation and the larger amount of partially oxidized products (such as CH_3SSCH_3) in the surface region of the sensing layer at 200°C than those at 300°C (see Fig. 5). Namely, the increase in the thickness of the sensing layer increased the amount of positively charged adsorption of CH_3SH and CH_3SSCH_3 on the bottom part of the sensing layer, which resulted in an increase in the CH_3SH response. However, the CH_3SH response of the *0.5*Ru/WO_3(*500*,*5*) sensor at 200°C was smaller than that observed at 300°C. This fact suggests the amount of CH_3SSCH_3 produced in the surface region of the sensing layer is quite small due to the thin sensing layer, and amount of positively charged adsorption of CH_3SSCH_3 on the bottom part of the sensing layer at 200°C was smaller than that at 300°C. Besides, the CH_3SH response of the *n*Ru/WO_3(*500*,*20*) sensors increased with an increase in the loading amount of Ru at 200°C and 300°C, and the effect of the Ru loading on the CH_3SH response at 200°C was larger than that at 300°C (see Fig. 3). This is probably because the amount of CH_3SSCH_3 produced at the bottom part of the sensing layer was increased by Ru loading onto WO_3. However, the CH_3SH response of the

*n*Ru/WO_3(*500*,*20*) sensors (*n* = *0*, *0.1* and *0.25*) at 300°C was larger than those at 200°C due to the large contribution of consumption of negatively adsorbed oxygen by the reaction with CH_3SH on the bottom part of the sensing layer. The CH_3SH response of the *n*Ru/WO_3(*500*,*20*) sensor at 400°C was smaller than that at 200°C or 300°C, probably because the large amount of CH_3SH oxidized in the surface region of the sensing layer at 400°C in comparison with those observed at lower temperatures. On the other hand, the CH_3SH response of the *0.5*Ru/WO_3(*400*,*27*) sensor was larger than that of the *0.5*Ru/WO_3(*500*,*50*) sensor (see Figs. 2 and 4). This fact means the SSA of the sensing layer also has a large impact on the diffusivity and reactivity of CH_3SH in the sensing layer.

To increase the porosity of the sensing layer and then improve the diffusivity of CH_3SH as well as CH_3SSCH_3 in the sensing layer, the sensing layers were fabricated by screen printing employing the pastes containing PMMA microspheres as a template. The surface and cross-sectional SEM photographs of representative p-*0.5*Ru/WO_3(*500*,*t*) sensors are depicted in Fig. 7. The thickness of the sensing layers increased with an increase in the number of the screen printing. In addition, homogeneous porous structures with a size of 100–200 nm in diameter, which originated from the morphology of PMMA microspheres, were observed on the surface and the cross-sectional view of the sensing layer. In addition, any cracks in the sensing layer were not observed, probably because the sintering among WO_3-particles was suppressed in the heat-treatment process for the sensor fabrication, due to the well-developed porous structure derived from PMMA microspheres. Figure 8 shows typical response transients to 0.5 ppm CH_3SH of the p-*0.5*Ru/WO_3(*500*,*40*) and *0.5*Ru/WO_3(*500*,*36*) sensors and variations in response of the p-*0.5*Ru/WO_3(*500*,*t*) sensors to 0.5 ppm CH_3SH with the thickness of the sensors at 150 and 200°C. The resistance in base air largely increased with an increase in the porosity of the sensing layer at both operating temperatures. The CH_3SH response of the *0.5*Ru/WO_3(*500*,*40*) sensor was comparable to that of the p-*0.5*Ru/WO_3(*500*,*36*) sensor at 200°C, while the CH_3SH response of the p-*0.5*Ru/WO_3(*500*,*40*) sensor was obviously larger than that of the *0.5*Ru/WO_3(*500*,*36*) sensor at 150°C. Generally, the gas diffusivity decreases with a decrease in the operating temperature. However, many submicron-sized cracks were in the sensing layers of the *0.5*Ru/WO_3(*T*,*t*) sensors. Thus, CH_3SH can easily diffuse though these cracks to the

bottom part of the sensing layers. On the other hand, CH_3SH diffused only through the porous structure well-developed in the sensing layer, as for the p-*0.5*Ru/WO_3(*500*,*40*) sensor. Therefore, the large amount of partially oxidized products such as CH_3SSCH_3 were effectively produced in the surface region of the sensing layer of the p-*0.5*Ru/WO_3(*500*,*40*) sensor at 150°C, and most of them could easily reach to the bottom part of the sensing layer than that of the *0.5*Ru/WO_3(*500*,*36*) sensor, leading to the large CH_3SH response of the p-*0.5*Ru/WO_3(*500*,*40*) sensor at 150°C. These results probably indicate that the positively charged adsorption of partially oxidized products such as CH_3SSCH_3 on the bottom part of the sensing layer is effective in enhancing the CH_3SH response at 150°C. The CH_3SH response of the p-*0.5*Ru/WO_3(*500*,*t*) sensors increased with an increase in the thickness of the sensing layer at both temperatures, and the CH_3SH response at 150°C was much larger than that at 200°C. This is probably because the large amount of partially oxidized products was positively adsorbed on the bottom part of the sensing layer especially at 150°C, and the hypothesis is supported by the fact that the larger amount of CH_3SSCH_3 was produced over *0.5*Ru/WO_3 powders at 150°C than that at 200°C (see Fig. 5).

The effects of the lamination of the *0.5*Ru/WO_3(*500*,*20*) sensor with a catalytic layer on the CH_3SH-sensing properties were also investigated in this study. Table 1 summarizes the CH_3SH responses of the M//N//*0.5*Ru/WO_3(*500*,*20*) and N//*0.5*Ru/WO_3(*500*,*20*) sensors, together with their composition, and Fig. 9 shows response transients of these sensors to 0.5 ppm CH_3SH at 200°C. All the sensors showed larger CH_3SH responses than that of the *0.5*Ru/WO_3(*500*,*20*) sensor, probably due to the production of partially oxidized products such as CH_3SSCH_3 in the catalytic layer and positively charged adsorption thereof on the bottom part of the sensing layer. The lamination of the *0.5*Ru/WO_3(*500*,*20*) sensor with only a Al_2O_3 layer largely enhanced the CH_3SH response, while the further lamination of the Al_2O_3//*0.5*Ru/WO_3(*500*,*20*) sensor with a *m*Pd/Al_2O_3 layer was not effective in improving the CH_3SH response. It is expected that the catalytic activity of Al_2O_3 is generally much smaller than those of these *m*Pd/Al_2O_3. Therefore, the large amount of CH_3SH was effectively oxidized in the *m*Pd/Al_2O_3 layer, and thus the small amount of CH_3SH and partially oxidized products such as CH_3SSCH_3 reached the bottom part of the sensing layer, to show the small CH_3SH responses.

On the other hand, the lamination of the sensing layer with only an Al_2O_3 layer is considered to be suitable for the enhancement of the CH_3SH response, because the poor catalytic activity of the Al_2O_3 for CH_3SH oxidation probably enhanced the production of the partially oxidized products such as CH_3SSCH_3 and the positively charged adsorption on the sensing layer.

Conclusion

The CH_3SH-sensing properties of WO_3-based semiconductor-type gas sensors were examined and factors for enhancing the CH_3SH-sensing properties were discussed. The Ru loading on WO_3 improved the CH_3SH response, and the CH_3SH response of the *n*Ru/WO_3(*T*,*t*) sensors increased with a decrease in the operating temperature as well as with an increase in the thickness of the sensing layer. In addition, the calcination temperature of the *0.5*Ru/WO_3 powders also affects the CH_3SH response. The *0.5*Ru/WO_3(*400*,*27*) sensor showed the largest CH_3SH response among the *n*Ru/WO_3(*T*,*t*) sensors.

Catalytic combustion behavior of 80 ppm CH_3SH over the *0.5*Ru/WO_3 powder was higher than that of the WO_3 powder, and the large amount of CH_3SSCH_3 generated at around 175°C and 125°C for WO_3 and *0.5*Ru/WO_3 powders, respectively. The obtained results suggested that the consumption of negatively adsorbed oxygen by the reaction with CH_3SH and CH_3SSCH_3 and the increase in positively charged adsorption of CH_3SH and CH_3SSCH_3 on the bottom part of the sensing layer synergistically contribute to the improvement in the CH_3SH response.

Introducing a porous structure employing PMMA microspheres into the *0.5*Ru/WO_3 sensing layer largely enhanced the CH_3SH response at 150°C, and the p-*0.5*Ru/WO_3(*500*,*54*) sensor operated at 150°C showed the largest CH_3SH response among all the sensors examined. In addition, the *0.5*Ru/WO_3(*500*,*20*) sensor laminated with catalytic layers also showed relatively large CH_3SH response, and the lamination of the *0.5*Ru/WO_3(*500*,*20*) sensor with an Al_2O_3 layer was the most effective in enhancing the CH_3SH response. These results indicate that the positively charged adsorption of the partially oxidized products onto the bottom part of the sensing layer is one of the important factors to obtain the large CH_3SH response, especially at lower operating temperatures.

Table 1

Sensor No.			1	2	3	4
Catalytic layer	Upper	*n*Pd/α-Al_2O_3	−	−	○ (*n=0.5*)	○ (*n=1.0*)
	Lower	α-Al_2O_3	−	○	○	○
Sensing layer		*0.5*Ru/WO_3(*500*,*20*)	○	○	○	○
		R_s	1.87	3.09	2.47	2.09

References

[1] W.-T. Koo, S.-J. Choi, N.-H. Kim, J.-S. Jang, I.-D. Kim, Catalyst-decorated hollow WO_3 nanotubes usinglayer-by-layer self-assembly on polymeric nanofiber templates and their application in exhaled breath sensor, Sens. Actuators B, 223 (2016) 301–310.

[2] C. Deng, J. Zhang, X. Yu, W. Zhang, X. Zhang, Determination of acetone in human breath by gas chromatography–mass spectrometry and solid-phase microextraction with on-fiber derivatization, J. Chromatogr. B, 810(2) (2004) 269–275.

[3] S. Dubois, S. Eng, R. Bhattacharya, S. Rulyak, T. Hubbard, D. Putnam, D. Kearney, Breath ammonia testing for diagnosis of hepatic encephalopathy, Dig. Dis. Sci. 50 (2005) 1780–1784.

[4] D. D. Vuong, G. Sakai, K. Shimanoe, N. Yamazoe, Hydrogen sulfide gas sensing properties of thin films derived from SnO_2 sols different in grain size, Sens. Actuators B, 105 (2005) 437–442.

[5] C. O. Park, S. A. Akbar, Ceramics for chemical sensing, J. Mater. Sci. 38 (2003) 4611–4637.

[6] K. Wetchakun, T. Samerjai, N. Tamaekong, C. Liewhiran, C. Siriwong, V. Kruefu, A. Wisitsoraat, A. Tuantranont, S. Phanichphant, Semiconducting metal oxides as sensors for environmentally hazardous gases, Sens. Actuators B. 160 (2011) 580–591.

[7] K. Yaegaki, K. Sanada, Volatile sulfur compounds in mouth air from clinically healthy subjects and patients with periodontal disease et al., J. Periodont. Res., 27 (1992) 233–238.

[8] M. Ando, S. Suto, T. Suzuki, T. Tsuchida, C. Nakayama, N. Miura, N. Yamazoe, H_2S and CH_3SH sensor using a thick film of gold-loaded tungsten oxide, Chem. Lett., 23(2) (1994) 335–338.

[9] S.-J. Kim, S.-J. Choi, J.-S. Jang, N.-H. Kim, M. Hakim, H. L. Tuller, I.-D. Kim, Mesoporous WO_3 nanofibers with protein-templated nanoscale catalysts for detection of trace biomarkers in exhaled breath, ACS Nano, 10 (2016) 5891–5899.

[10] X. Chu, P. Siciliano, CH_3SH-sensing characteristics of $LaFeO_3$ thick-film prepared by co-precipitation method, Sens. Actuators B 94 (2003) 197–200.

[11] X. Chu, Dilute CH_3SH-sensing characteristics of $BaSnO_3$ thick film sensor, Mater. Sci. Eng. B-Solid State Mater. Adv. Technol., 106 (2004) 305–307.

[12] Y. Shimizu, S. Kai, Y. Takao, T. Hyodo, M. Egashira, Correlation between methylmercaptan gas-sensing properties and its surface chemistry of SnO_2-based sensor materials, Sensors and Actuators B 65 (2000) 349–357.

[13] R. Ionescu, A. Hoel, C.G. Granqvist, E. Llobet, P. Heszler, Low-level detection of ethanol and H_2S with temperature-modulated WO_3 nanoparticle gas sensors, Sens. Actuators B 104 (2005) 132–139.

[14] C. S. Rout, M. Hegde, C.N.R. Rao, H_2S sensors based on tungsten oxide nanostructures, Sens. Actuators B 128 (2008) 488–493.

[15] N. –H. Kim, S. –J. Choi, D. –J. Yang, J. Bae, J. Park, I. –D. Kim, Highly sensitive and selective hydrogen sulfide and toluene sensors using Pd functionalized WO_3 nanofibers for potential diagnosis of halitosis and lung cancer, Sen. and Actuators B 193 (2014) 574–581.

[16] S. Bai, K. Zhang, J. Sun, D. Zhang, R. Luo, D. Li, C. Liu, Polythiophene-WO_3 hybrid architectures for low-temperature H_2S detection, Sens. Actuators B 197 (2014) 142–148.

[17] Y. Shen, B. Zhang, X. Cao, D. Wei, J. Ma, L. Jia, S. Gao, B. Cui, Y. Jin, Microstructure and enhanced H_2S sensing properties of Pt-loaded WO_3 thin films, Sens. and Actuators B 193 (2014) 273–279.

[18] L. Yin, D. Chen, H. Zhang, G. Shao, B. Fan, R. Zhang, G. Shao, In situ formation of Au/SnO_2 nanocrystals on WO_3 nanoplates as excellent gas-sensing materials for H_2S detection, Mater. Chem. Phys., 148 (2014) 1099–1107.

[19] Lee, S.-J. Choi, K.-M. Park, S. S. Lee, S. Choi, I.-D. Kim, C. O. Park, The stability, sensitivity and response transients of ZnO, SnO_2 and WO_3 sensors under acetone, toluene and H_2S environments, Sens. Actuators B, 197 (2014) 300–307.

[20] V. Kruefu, A. Wisitsoraatb, A. Tuantranontb, S. Phanichphantca, Ultra-sensitive H_2S sensors based on hydrothermal/impregnation-made Ru-functionalized WO_3 nanorods, Sens. Actuators B, 215 (2015) 630–636.

[21] Y. Takao, M.-H. Han, Y. Shimizu, M. Egashira, Effect of sensor thickness on trimethylamine sensitivity of In_2O_3-MgO sensors loaded with noble metals, Denki Kagaku (presently, Electrochemistry), 64 (1996) 1280–1284.

[22] Kawahara, K. Yoshihara, H. Katsuki, Y. Shimizu, M. Egashira, Gas-sensing properties of semiconductor heterolayers fabricated by a slide-off transfer printing method, Sens. Actuators B, 65 (2000) 17–22.

[23] Y. Shimizu, M. Egashira, Basic aspects and challenges of semiconductor gas sensors, MRS Bull., 24 (1999) 18–24.

[24] T. Hyodo, Y. Tominaga, T. Yamaguchi, A. Kawahara, H. Katsuki, Y. Shimizu, M. Egashira, NOx sensing properties of WO3-based semiconductor gas sensors fabricated by slide-off transfer printing, Electrochemistry, 71 (2003) 481–484.

[25] T. Hyodo, N. Nishida, Y. Shimizu, M. Egashira, Preparation and gas-sensing properties of thermally stable mesoporous SnO_2, Sens. Actuators B, 83 (2002) 209–215.

[26] T. Hyodo, S. Abe, Y. Shimizu, M. Egashira, Gas-sensing properties of ordered mesoporous SnO_2 and effects of coating thereof, Sens. Actuators B, 93 (2003) 590–600.

[27] T. Hyodo, K. Sasahara, Y. Shimizu, M. Egashira, Preparation of macroporous SnO_2 films using PMMA microspheres and their sensing properties to NOx and H_2, Sens. Actuators B, 106 (2005) 580–590.

[28] K. Hieda, T. Hyodo, Y. Shimizu, M. Egashira, Preparation of porous tin dioxide powder by ultrasonic spray pyrolysis and their application to sensor materials, Sens. Actuators B, 133 (2008) 144–150.

[29] T. Hyodo, E. Fujii, K. Ishida, T. Ueda, Y. Shimizu, Microstructural control of porous In_2O_3 powders prepared byultrasonic-spray pyrolysis employing self-synthesized polymethylmethacrylate microspheres as a template and their NO_2-sensing properties, Sens. Actuators B, 244 (2017) 992–1003.

[30] Y. Yuzuriha, T. Hyodo, T. Sasahara, Y. Shimizu, M. Egashira, Mesoporous Al_2O_3 Co-loaded with Pd and Au as a combustion catalyst for adsorption/combustion-type gas sensors, Sens. Lett., 9 (2011) 1–5.

[31] C. W. Walter, C. F. Hertzler, P. Devynck, G. P. Smith, J. R. Peterson, Photodetachment of WO_3^-: The electron affinity of WO_3, J. Chem. Phys., 95 (1991) 824–827.

[32] Y. –L. Chueh, C. –H. Hsieh, M. –T. Chang, L. –J., Chou, C. S. Lao, J. H. Song, J.-Y. Gan, Z. L. Wang, RuO_2 Nanowires and RuO_2/TiO_2 core/shell nanowires: from synthesis to mechanical, Optical, Electrical, and Photoconductive Properties, Adv. Mater., 19 (2007) 143–149.

Figure captions

Fig. 1. (a)–(e) Cross-sectional views of the sensing layers of representative *0.5*Ru/WO_3(*500*,*t*) sensors together with their thickness, and (f) surface view of the sensing layer of the *0.5*Ru/WO_3(*500*,*32*) sensor. Fabrication method was shown as "sc(*N*)" for screen printing (*N*: the number of screen printing) or "applying" in brackets.

Fig. 2. Variations in response of the *0.5*Ru/WO_3(*500*,*t*) sensors to 0.5 ppm CH_3SH with the thickness of the sensing layer in wet air (65%RH at 20°C) at 200, 300 and 400°C.

Fig. 3. Response transients of the *n*Ru/WO_3(*500*,*20*) sensors to 0.5 ppm CH_3SH in wet air (65%RH at 20°C) at 200, 300 and 400°C.

Fig. 4. Variations in response of the *0.5*Ru/WO_3(*T*,*t*) sensors to 0.5 ppm CH_3SH in wet air (65%RH at 20°C) at 200°C and specific surface areas (SSAs) of the WO_3 powders with the calcination-temperature, together with layer thickness of the sensors.

Fig. 5. Temperature dependence of conversion of 80 ppm CH_3SH balanced with wet air (65%RH at 20°C) together with relative amounts of products by the oxidation of CH_3SH over WO_3 and *0.5*Ru/WO_3 powders.

Fig. 6. Schematic view of a CH_3SH-sensing mechanism of the WO_3-based sensors.

Fig. 7. (a)–(c) Cross-sectional views of the sensing layers of representative p-*0.5*Ru/WO_3(*500*,*t*) sensors together with their thickness, (d) surface view of the p-*0.5*Ru/WO_3(*500*,*40*) sensor as a representative of the *0.5*Ru/WO_3(*500*,*t*) sensors. Fabrication method was shown as "sc(*N*)" for screen printing (*N*: the number of screen printing).

Fig. 8. (a) and (b) Response transients of the *n*Ru/WO_3(*500*,*36*) and p-*0.5*Ru/WO_3(500,*40*) sensors to 0.5 ppm CH_3SH in wet air (65%RH at 20°C) at 150°C, respectively, and (c) variations in CH_3SH response of the p-*0.5*Ru/WO_3(*500*,*t*) sensors with the thickness of the sensing layer in wet air (65%RH at 20°C) at 150 and 200°C.

Fig. 9. Response transients of the α-Al_2O_3//*0.5*Ru/WO_3 and *m*Pd/α-Al_2O_3//α-Al_2O_3//*0.5*Ru/WO_3 sensors laminated with catalytic layers to 0.5 ppm CH_3SH in wet air (65%RH at 20°C) at 200, 300 and 400°C.

Table 1 Comparison of response of the *0.5*Ru/WO_3(*500*,*20*) sensors to 0.5 ppm CH_3SH laminated with catalytic layers together with the composition of these sensors.

Fig. 1

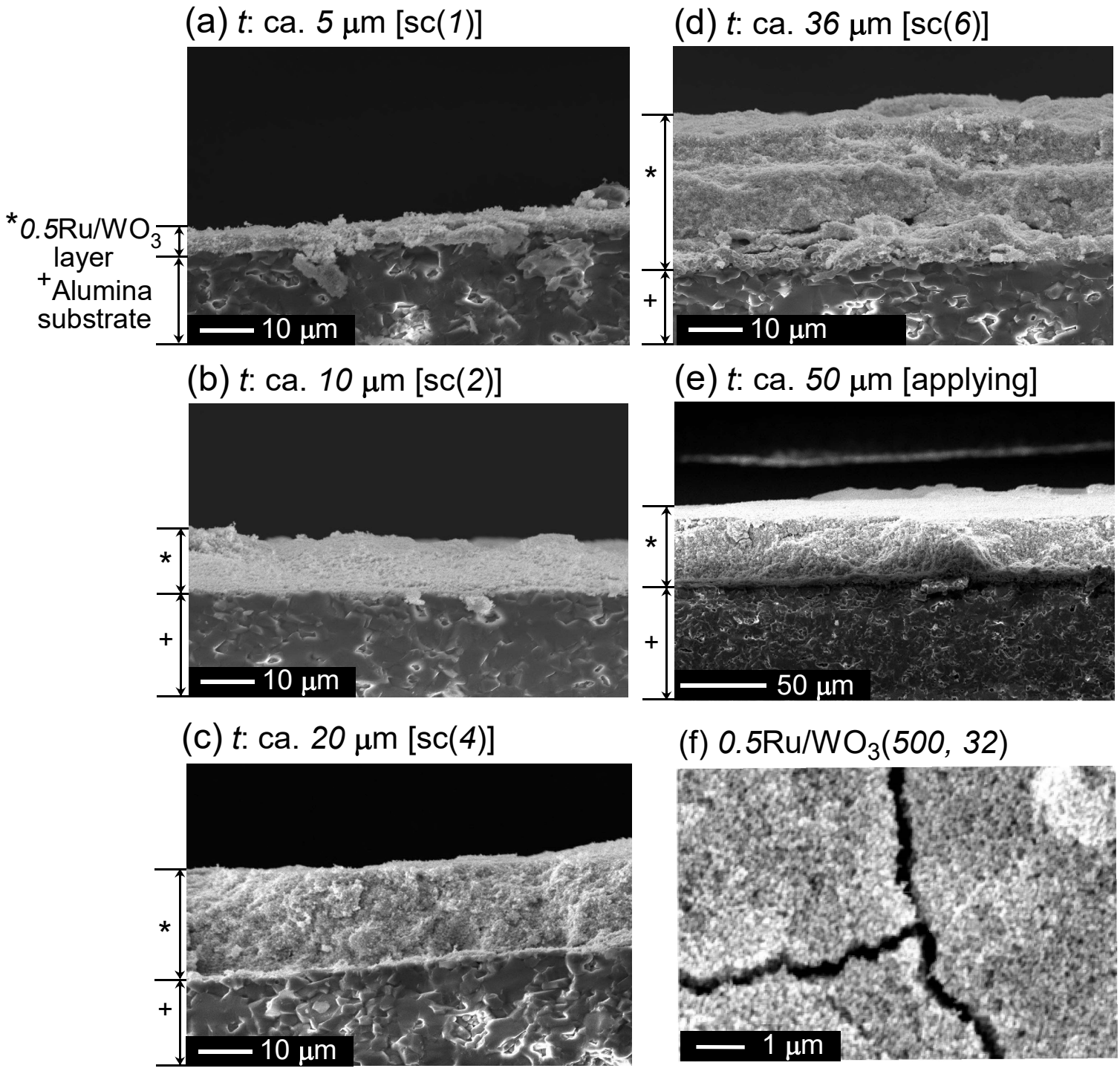
(a) t: ca. 5 μm [sc(1)]
(d) t: ca. 36 μm [sc(6)]
*0.5Ru/WO3 layer
+Alumina substrate
10 μm
10 μm
(b) t: ca. 10 μm [sc(2)]
(e) t: ca. 50 μm [applying]
10 μm
50 μm
(c) t: ca. 20 μm [sc(4)]
(f) 0.5Ru/WO3(500, 32)
10 μm
1 μm

Fig. 2

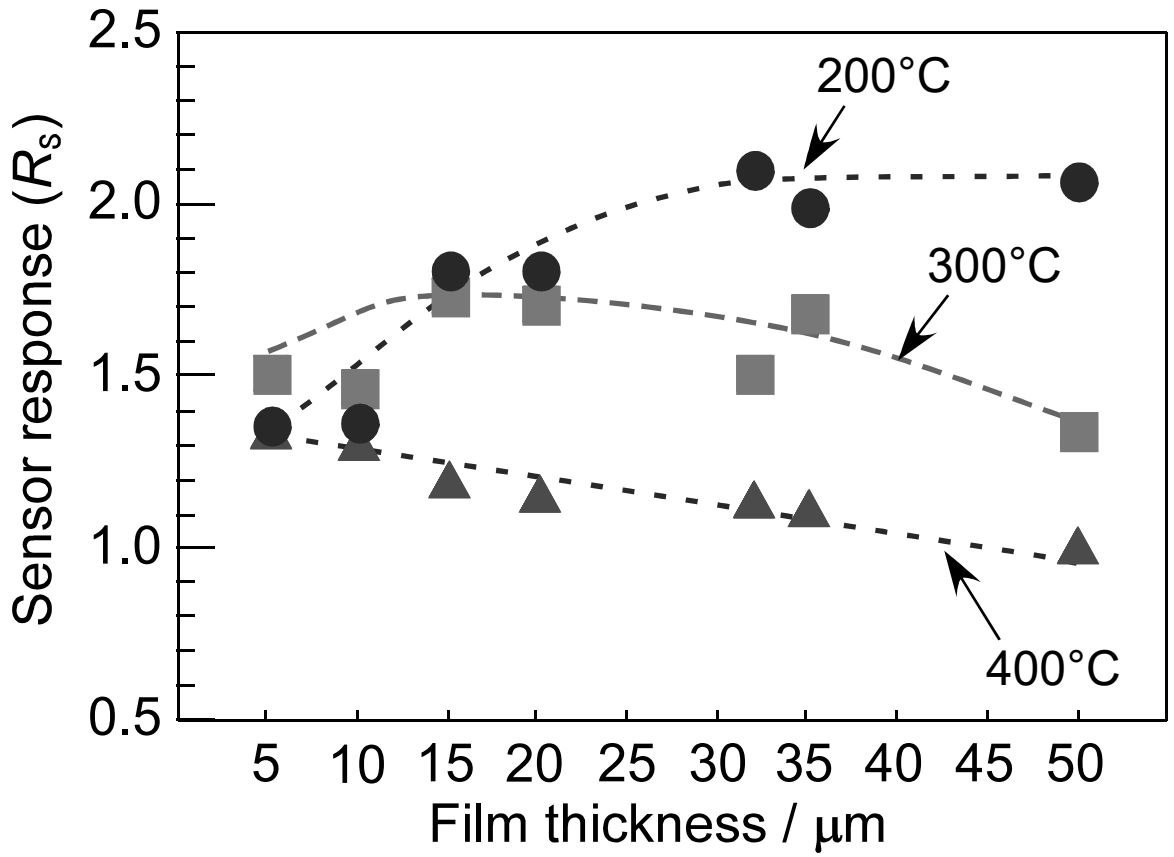
Sensor response (R_s)
2.5
2.0
1.5
1.0
0.5
5
10
15
20
25
30
35
40
45
50
Film thickness / μm
200°C
300°C
400°C

Fig. 3

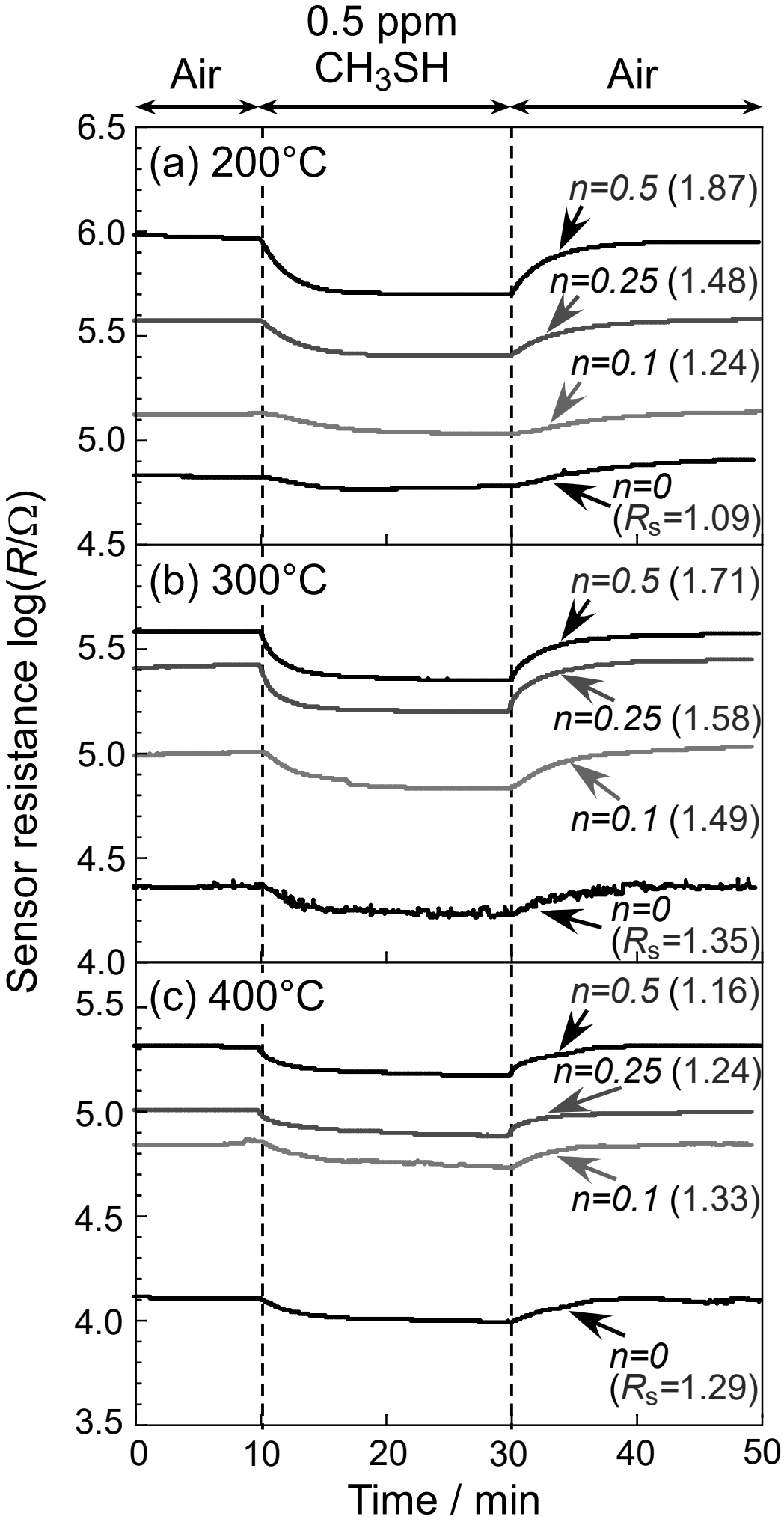
0.5 ppm
CH3SH
Air
Air
(a) 200°C
n=0.5 (1.87)
n=0.25 (1.48)
n=0.1 (1.24)
n=0
(Rs=1.09)
(b) 300°C
n=0.5 (1.71)
n=0.25 (1.58)
n=0.1 (1.49)
n=0
(Rs=1.35)
(c) 400°C
n=0.5 (1.16)
n=0.25 (1.24)
n=0.1 (1.33)
n=0
(Rs=1.29)
Sensor resistance log(R/Ω)
Time / min
6.5
6.0
5.5
5.0
4.5
5.5
5.0
4.5
4.0
5.5
5.0
4.5
4.0
3.5
0
10
20
30
40
50

Fig. 4

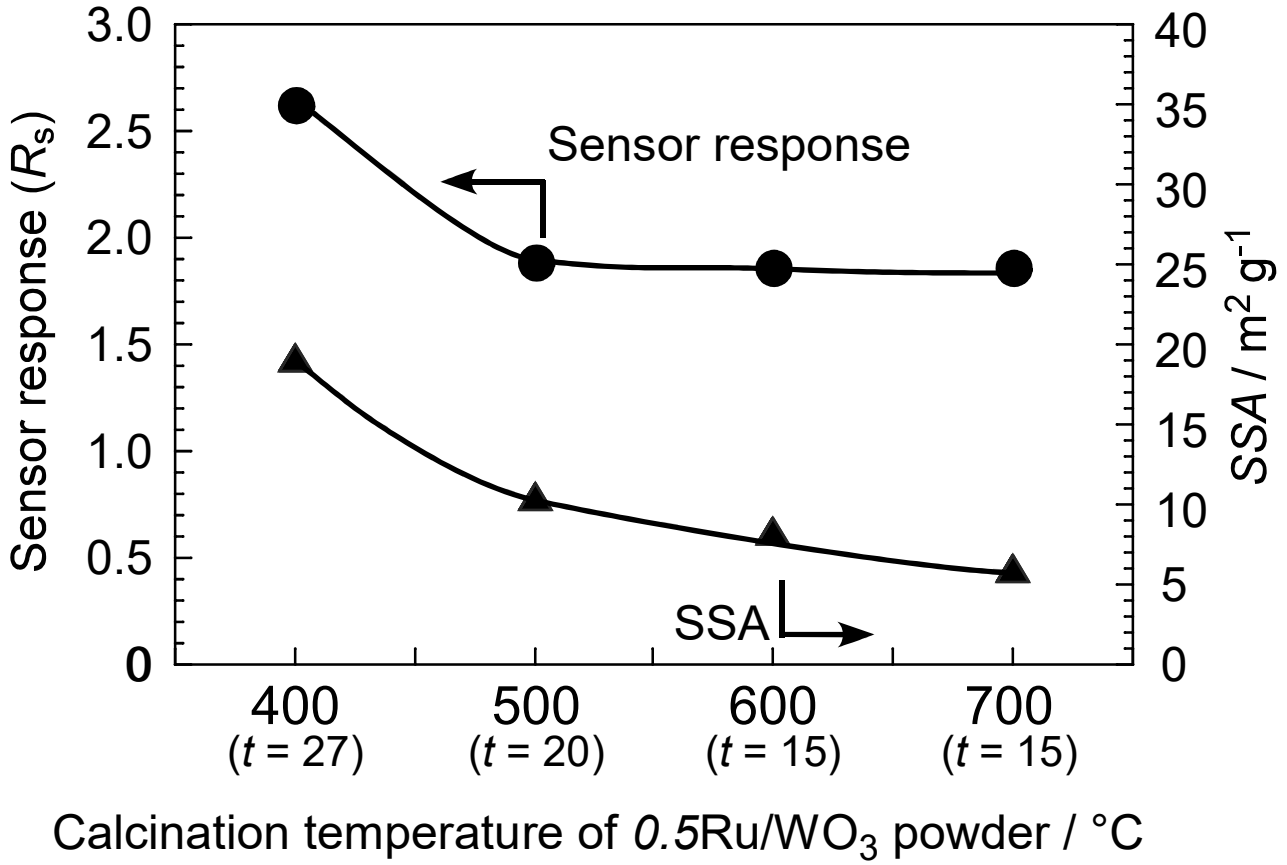
Sensor response (R_s)
3.0
2.5
2.0
1.5
1.0
0.5
0
Sensor response
SSA
40
35
30
25
20
15
10
5
0
SSA / m^2 g^{-1}
400
(t = 27)
500
(t = 20)
600
(t = 15)
700
(t = 15)
Calcination temperature of *0.5*Ru/WO_3 powder / °C

Fig. 5

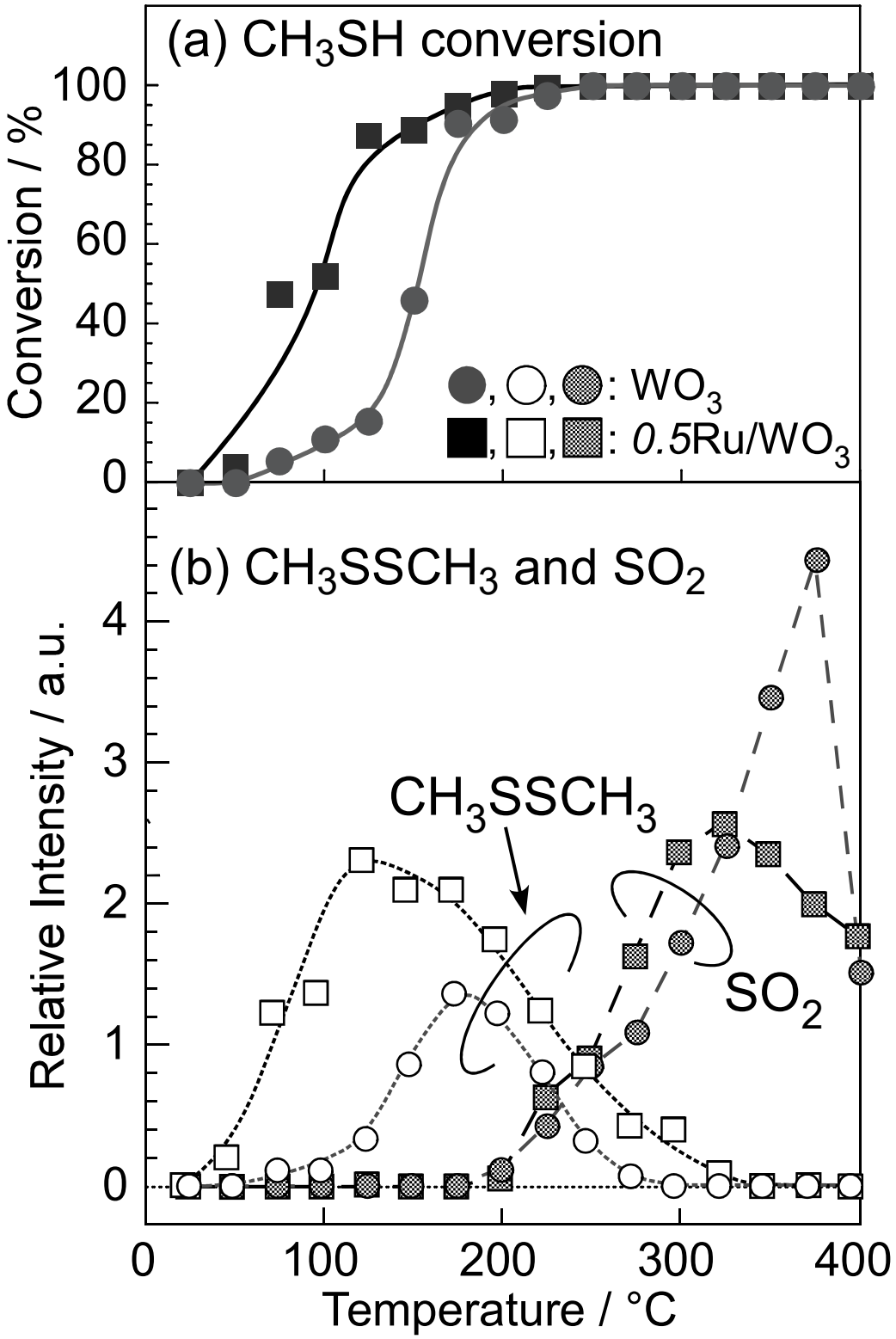
(a) CH_3SH conversion
Conversion / %
100
80
60
40
20
0
●, ○, ▨: WO_3
■, □, ▩: *0.5*Ru/WO_3
(b) CH_3SSCH_3 and SO_2
Relative Intensity / a.u.
4
3
2
1
0
CH_3SSCH_3
SO_2
0
100
200
300
400
Temperature / °C

Fig. 6

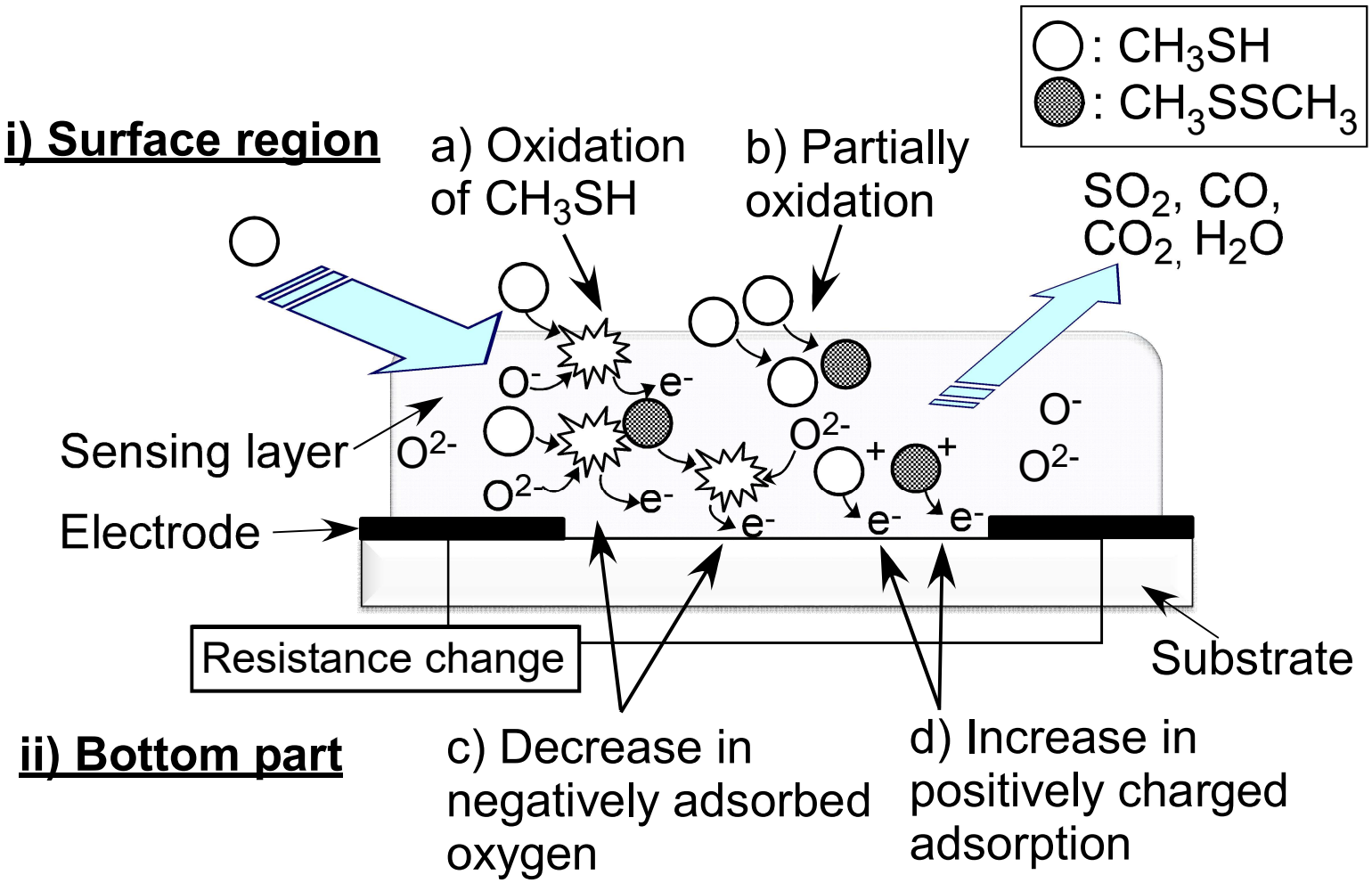
: CH_3SH
: CH_3SSCH_3
i) Surface region
a) Oxidation of CH_3SH
b) Partially oxidation
SO_2, CO, CO_2, H_2O
Sensing layer
Electrode
Resistance change
Substrate
ii) Bottom part
c) Decrease in negatively adsorbed oxygen
d) Increase in positively charged adsorption

Fig. 7

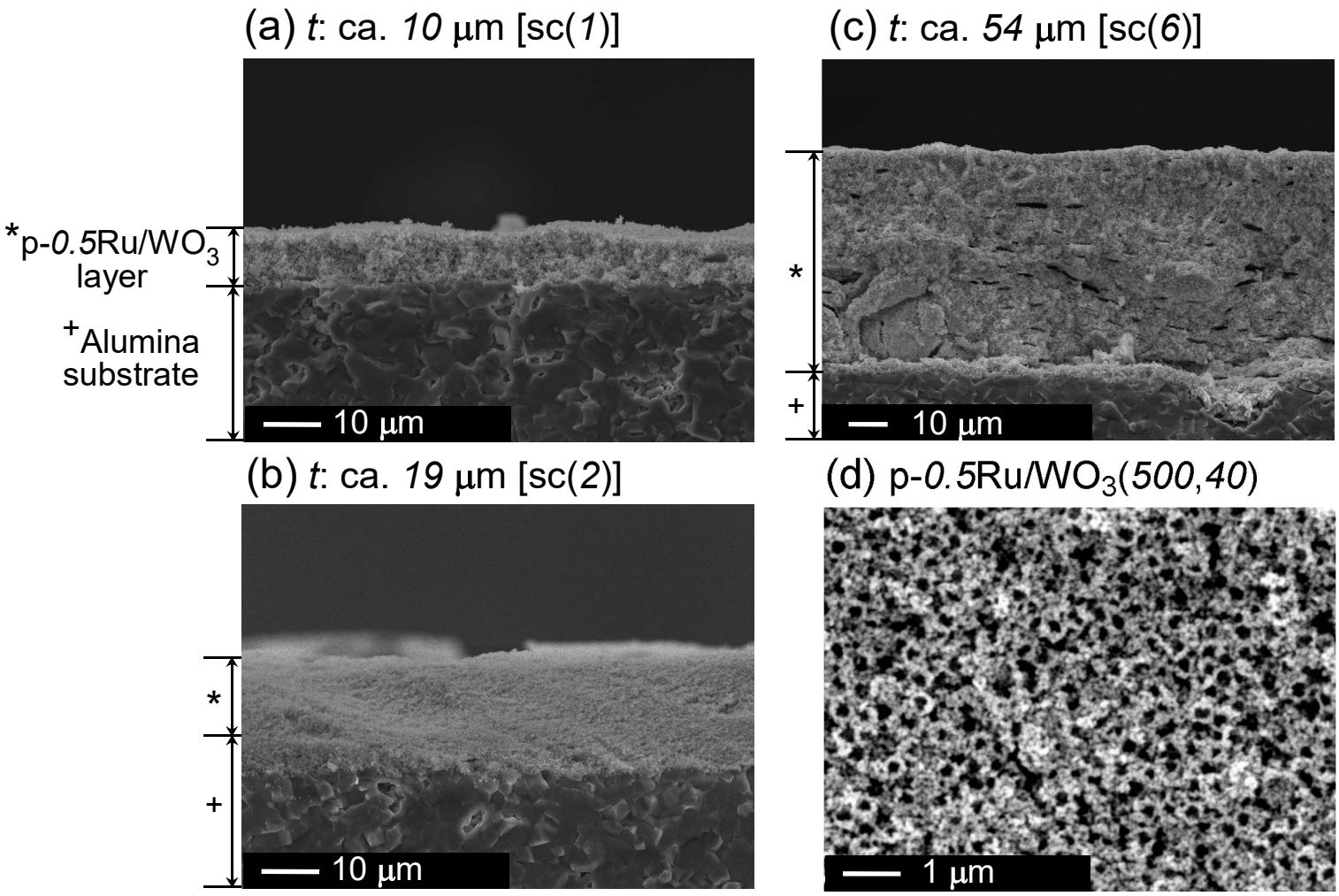
(a) t: ca. 10 μm [sc(1)]
*p-0.5Ru/WO3 layer
+Alumina substrate
10 μm
(c) t: ca. 54 μm [sc(6)]
*
+
10 μm
(b) t: ca. 19 μm [sc(2)]
*
+
10 μm
(d) p-0.5Ru/WO3(500,40)
1 μm

Fig. 8

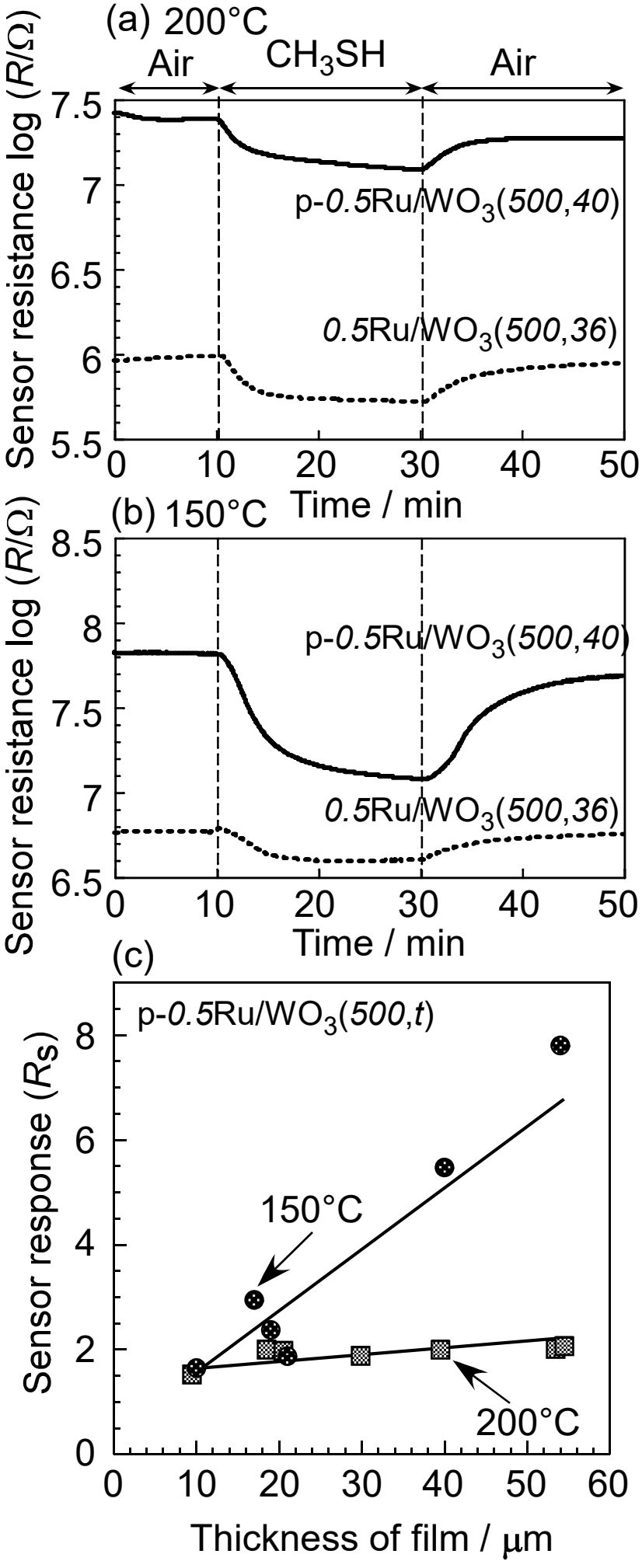
(a) 200°C
Air
CH_3SH
Air
Sensor resistance log (R/Ω)
p-*0.5*Ru/WO_3(*500*,*40*)
*0.5*Ru/WO_3(*500*,*36*)
Time / min
(b) 150°C
Sensor resistance log (R/Ω)
p-*0.5*Ru/WO_3(*500*,*40*)
*0.5*Ru/WO_3(*500*,*36*)
Time / min
(c)
p-*0.5*Ru/WO_3(*500*,*t*)
Sensor response (R_S)
150°C
200°C
Thickness of film / μm

Fig. 9

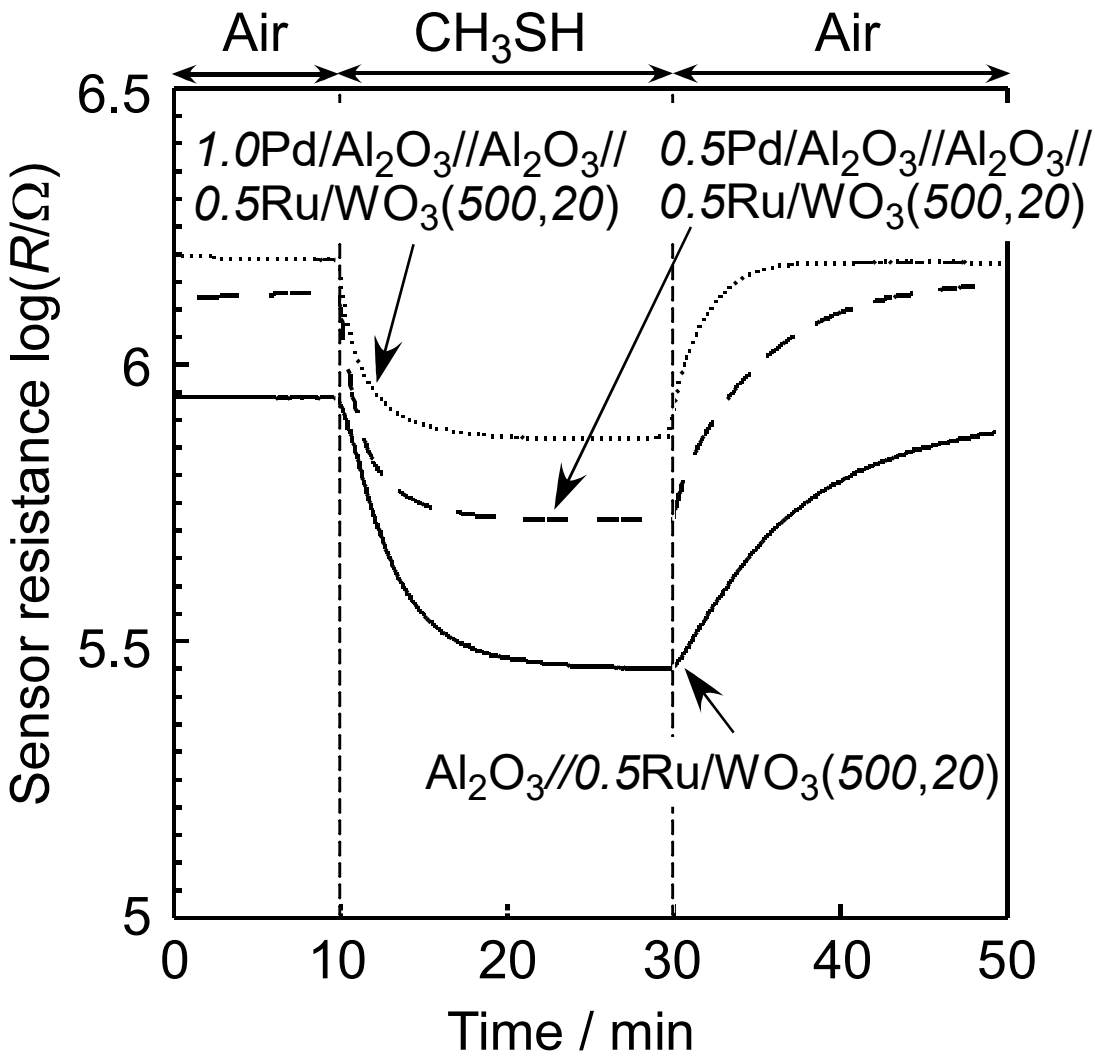
Air
CH3SH
Air
6.5
6
5.5
5
0
10
20
30
40
50
Sensor resistance log(R/Ω)
Time / min
1.0Pd/Al2O3//Al2O3//
0.5Ru/WO3(500,20)
0.5Pd/Al2O3//Al2O3//
0.5Ru/WO3(500,20)
Al2O3//0.5Ru/WO3(500,20)